MATERIALS SCIENCE

Electronic Raman scattering in the 2D antiferromagnet $NiPS_3$

Xingzhi Wang[1]*†, Jun Cao[1], Hua Li[2], Zhengguang Lu[3,4], Arielle Cohen[5], Anubhab Haldar[5], Hikari Kitadai[1], Qishuo Tan[1], Kenneth S. Burch[6], Dmitry Smirnov[3], Weigao Xu[2], Sahar Sharifzadeh[1,5,7,8], Liangbo Liang[9], Xi Ling[1,5,10]*

Correlated-electron systems have long been an important platform for various interesting phenomena and fundamental questions in condensed matter physics. As a pivotal process in these systems, *d-d* transitions have been suggested as a key factor toward realizing optical spin control in two-dimensional (2D) magnets. However, it remains unclear how *d-d* excitations behave in quasi-2D systems with strong electronic correlation and spin-charge coupling. Here, we present a systematic electronic Raman spectroscopy investigation on *d-d* transitions in a 2D antiferromagnet—$NiPS_3$, from bulk to atomically thin samples. Two electronic Raman modes originating from the scattering of incident photons with *d* electrons in Ni^{2+} ions are observed at ~1.0 eV. This electronic process persists down to trilayer flakes and exhibits insensitivity to the spin ordering of $NiPS_3$. Our study demonstrates the utility of electronic Raman scattering in investigating the unique electronic structure and its coupling to magnetism in correlated 2D magnets.

INTRODUCTION

Van der Waals (vdW) magnetic materials have received growing interest revealing physics in the extreme nanoscale limit (*1*–*5*). Recently, attentions have been focused on a antiferromagnet, nickel phosphorus trisulfides ($NiPS_3$), due to its intriguing physics in quasi two-dimensional (2D) systems, including phonon-magnon coupling (*6*), strong electron correlation (*7*), and spin-correlated excitonic physics (*8*–*10*). As a 2D magnet with strongly correlated *d* electrons, *d-d* transition in $NiPS_3$ plays an important role in determining and controlling spin properties (*11*, *12*). For example, light-induced magnetic anisotropy has been demonstrated in $NiPS_3$ by optically pumping the *d* electrons to the higher-energy orbital states of Ni^{2+} ions (*11*). Despite extensive interest in low-dimensional correlated systems, it is notable that few studies have focused on *d-d* excitations in atomically thin vdW layers (*13*–*15*). The *d-d* excitations in 2D layers are expected to be different from that in the bulk cases, because the onsite coulomb repulsion (Hubbard *U*) can be modified by the increasing dielectric screening (*16*). However, because of the forbidden selection rule, the absorptions corresponding to the *d-d* transitions in $NiPS_3$ are much weaker compared to the interband transitions and generally become undetectable using absorption spectroscopy in the thin layers (*7*). Such invisibility prevents the ability to uncover the subtle changes in the correlated *d* electron states in 2D systems.

Raman spectroscopy has been an effective optical tool with non-destructivity and high sensitivity in the study of elemental excitations, including phonons, excitons, polaritons, magnons, and spinons in condensed matter systems (*17*–*19*). The selection rule of Raman scattering offers great capabilities to reveal the symmetry and coupling to magnetism in various 2D magnets (*20*–*24*). Electronic Raman (ER) scattering, where photons are scattered by electronic excitations in the materials, has been used in revealing the electronic behaviors in low-dimensional materials, such as metallic carbon nanotubes and AlGaAs epilayers (*25*, *26*). $NiPS_3$ exhibits a unique electronic structure with a highly localized electronic band composed by *d* orbitals (*9*, *27*), suggesting a potential to explore the *d-d* transitions in 2D systems using ER spectroscopy.

Here, we present a systematic study on ER scattering in $NiPS_3$ layers and explore its origin and correlation with the spin structure. Two ER modes with energies around 1.0 eV have been observed far below the bandgap under a wide range of excitation from 454 to 531 nm in $NiPS_3$ down to few-layer flakes. Such ER scattering is attributed to the photon scattering by the *d-d* excitations, which represent electronic transition between *d* orbitals in Ni^{2+} ions. In contrast to the spin-correlated interband transitions, *d-d* transitions exhibit distinct independence on the formation of spin structure near Néel temperature (T_N) and on external magnetic field. Our study suggests the ER scattering to be a unique probe to reveal the electronic transitions related to *d* orbitals in 2D strong-correlated systems, which can provide rich physical information for the study of fundamental physics and the design of ultrathin opto-magneto devices.

RESULTS

$NiPS_3$ has been of interest for its realization of antiferromagnetic XXZ model on a honeycomb lattice (*28*, *29*). As temperature decreases across its T_N = ~ 152 K, $NiPS_3$ undergoes a magnetic phase transition from the paramagnetic to the antiferromagnetic phase (*28*). High-quality $NiPS_3$ single crystals were grown using a chemical vapor transport method (*30*). Monolayer $NiPS_3$ crystal has a hexagonal lattice structure with threefold rotation symmetry, which is broken by the monoclinic interlayer stacking order in few-layer and bulk cases (see Fig. 1A and fig. S1A). When the temperature is below its

[1]Department of Chemistry, Boston University, Boston, MA 02215, USA. [2]Key Laboratory of Mesoscopic Chemistry, School of Chemistry and Chemical Engineering, Nanjing University, Nanjing 210023, China. [3]National High Magnetic Field Laboratory, Tallahassee, FL 32310, USA. [4]Department of Physics, Florida State University, Tallahassee, FL 32306, USA. [5]Division of Materials Science and Engineering, Boston University, Boston, MA 02215, USA. [6]Department of Physics, Boston College, Chestnut Hill, MA 02467, USA. [7]Department of Electrical and Computer Engineering, Boston University, Boston, MA 02215, USA. [8]Department of Physics, Boston University, Boston, MA 02215, USA. [9]Center for Nanophase Materials Sciences, Oak Ridge National Laboratory, Oak Ridge, TN 37831, USA. [10]The Photonics Center, Boston University, Boston, MA 02215, USA.
*Corresponding author. Email: xzwang@bu.edu (X.W.); xiling@bu.edu (X.L.)
†Present address: Department of Physics, Xiamen Univeristy, Xiamen, 361005, China.

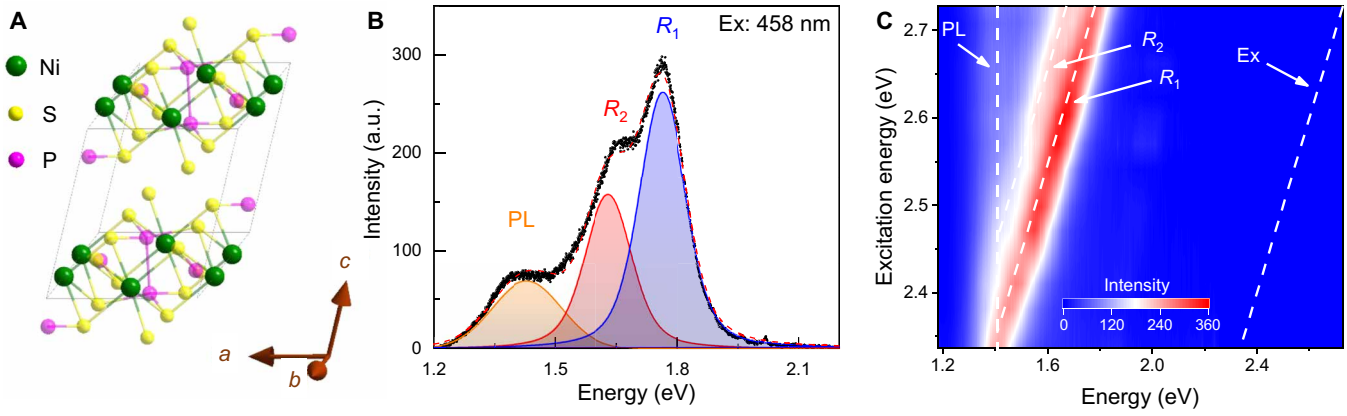

Fig. 1. ER spectra of vdW antiferromagnet $NiPS_3$. (**A**) Monoclinic crystal structure of $NiPS_3$. (**B**) Optical spectrum of bulk $NiPS_3$ excited by a 458-nm laser at 295 K. (**C**) Excitation (Ex)–dependent photoluminescence (PL) and ER map of $NiPS_3$. a.u., arbitrary units.

T_N, the spins form a zigzag antiferromagnetic order, where the intralayer spin moments are arranged ferromagnetically in chains but are coupled antiferromagnetically with their neighboring chains (see fig. S1B). The planes are also coupled ferromagnetically along the *c* direction. The spin direction in $NiPS_3$ is mainly along the *a* axis, with an angle of ~8° out of the *ab* plane (*29*).

Figure 1B displays a typical optical spectrum from an exfoliated thick $NiPS_3$ flake (~50 nm) under a 458-nm laser excitation at 295 K. The spectrum shows three peaks, ranging from the visible to the near infrared region. However, distinct spectra are obtained as the excitation wavelength varies from 454 nm (2.73 eV) to 531 nm (2.34 eV) (see Fig. 1C). In all the spectra under different laser excitations, a peak can be resolved at the same position ~1.39 eV, exhibiting a distinct feature of photoluminescence (PL). This peak could be assigned to the phonon sideband of the coherent Zhang-Rice exciton, which results in an ultrasharp and linear-polarized emission at low temperature (*9*, *10*). In contrast, the other two peaks, labeled as R_1 and R_2, exhibit an obvious redshift with the decrease of the excitation energy and, finally, disappear when the excitation energy is below ~2.35 eV. Each of the two peaks presents a fixed energy difference between the collected signal and the laser excitation, suggesting that their origin is Raman scattering rather than luminescence (see Fig. 2A).

Typically, Raman peaks in insulating magnets result from either phonons or magnons (*6*, *31*). However, these two types of excitations can be excluded as the origin of R_1 and R_2 in $NiPS_3$ based on multiple pieces of evidence. First, the Raman shifts of these two peaks are ~0.93 and 1.05 eV, which are much higher than the frequencies of phonon or magnon modes (*6*, *32*). Second, the observed Raman peaks have larger peak width of over 0.1 eV, in contrast to the narrow feature of one-phonon or one-magnon modes (*33*, *34*). In addition, the temperature- and polarization-dependent studies, which will be discussed in detail later, indicate that the behaviors of these two peaks are different from the two-magnon mode, which has been observed at 400 to 600 cm^{-1} in $NiPS_3$ (*6*). In contrast to the phonon and magnon modes, the large Raman shifts of the two peaks imply that they originate from electronic transitions. To confirm this, the electronic band structure and density of states for bulk $NiPS_3$ were calculated using first-principle density functional theory (DFT) + *U* method with $U = 4.0$ eV (see fig. S3) (*6*, *7*, *9*). The calculated band structure clearly shows the near-flat electronic bands near the conduction band minimum, which are predominantly contributed by Ni *d* orbitals (see fig. S3C). The small dispersion of these bands is due to the localization of the Ni *d* orbitals. In contrast, the valence bands are mostly from S *p* orbitals, leading to dispersive valance bands that are common in many other materials (see fig. S3D). The calculation indicates an indirect bandgap ~ 1.6 eV, which is consistent with the previous calculation and experimental measurements (*7*, *27*, *30*).

To reveal the origin of the two Raman peaks (i.e. R_1 and R_2), the absorbance measurement has been performed on thick $NiPS_3$ samples (see Fig. 2B). Different from most of traditional semiconductors, a distinct absorption feature is observed at ~1.0 eV, which is far below the reported bandgap at ~1.8 eV (*7*, *12*). This absorption can be resolved into two components with energies at ~0.92 and ~1.09 eV, in a good agreement with the Raman shifts of R_1 and R_2, suggesting that they originate from the same transition in the material. Such absorption was reported to result from *d*-*d* transitions on the transition metal ions in $NiPS_3$, as well as many other transition metal compounds (*14*, *35*–*37*). The nickel atom is located at the center of a trigonally distorted octahedral crystal field, constituting of six sulfur atoms (see Fig. 2C). As a result, the *d* orbitals of Ni^{2+} ion split into several states, among which the ground state $^3A_{2g}$ and the first excited state $^3T_{2g}$ are directly involved in the observed ER scattering with large Raman shift at ~1.0 eV (see Fig. 2D). Moreover, because of the trigonal distortion, the $^3T_{2g}$ state further splits into $^3A_{1g}$ and ^3E_g states, leading to the observation of two ER modes that correspond to the transition $^3A_{2g} \rightarrow {}^3A_{1g}$ and $^3A_{2g} \rightarrow {}^3E_g$. Note that DFT + *U* calculation does not reveal these features of *d* orbitals, instead predicting a charge transfer (*s*/*p* to *d*) transition at 1.45 eV. This discrepancy may be due to the fact that DFT + *U* may fail for describing certain physical properties of strongly correlated materials. This approach does not fully account for the multicorrelated nature of *d* orbitals (*38*, *39*); in addition, the lack of self-interaction error correction for *s*/*p* states and lack of excitonic effects can result in an error in the predicted nature of transitions (*37*, *38*). Considering the selection rule for angular momentum conservation, direct *d*-*d* transitions are generally forbidden, while it becomes allowed due to the vibronic coupling in materials (*13*, *40*).

The intensity of ER peaks exhibit a clear dependence on the excitation energy, indicating a resonant effect, which is related to an external electronic state as an intermediate state (see Fig. 2E). The ER intensity can be given by the formula as (*41*, *42*)

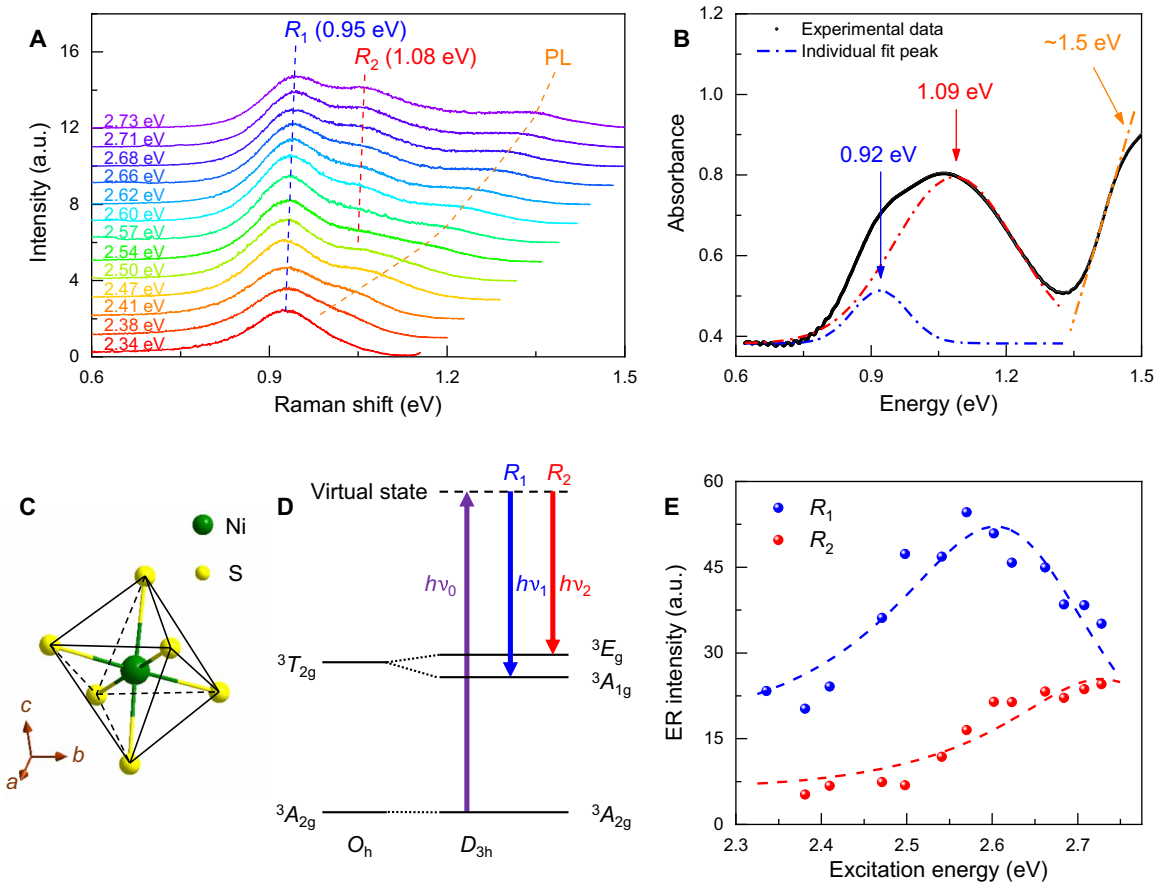

Fig. 2. Mechanism of ER modes in $NiPS_3$. (**A**) Optical spectra of $NiPS_3$ plotted in terms of Raman shift, i.e., energy difference from excitation energy, excited by different lasers with energies from 2.73 to 2.34 eV. (**B**) Absorption spectrum of bulk $NiPS_3$ below the main absorption edge (~1.5 eV), indicating a weak absorption feature consisting of two components. (**C**) Centered Ni^{2+} ion in a trigonally distorted octahedral sulfide environment. (**D**) Schematic illustration of ER scattering in between the ground state and first excited triplet state for Ni^{2+} ion in a trigonally distorted octahedral environment (D_{3h}). O_h represents the crystal field splitting in an octahedral field; $h\nu_0$ and $h\nu_1(h\nu_2)$ are the energy of incident and scattered photons of R_1 (R_2) mode. (**E**) Integrated intensity of two ER peaks as a function of excitation energy. The dashed lines are the fitting curves.

$$I(E_L) = \frac{A}{|(E_L - E_{mi} - i\Gamma)(E_L - E_{mi} - E_{ex} - i\Gamma)|^2}$$

where A is a constant related to the electron-photon coupling; E_L, E_{mi}, and E_{ex} are the incident photon energy, the intermediate state energy, and excited state energy, respectively; Γ is the damping constant. ER intensity will achieve a maximum when $E_L = E_{mi} + E_{ex}$. The intensities of ER modes, R_1 and R_2, reach the maximum at ~2.61 and ~2.73 eV, respectively. The different resonant energies of two modes indicate a scattered light resonance, where $E_L = E_{mi} + E_{ex}$. Therefore, E_{mi} can be obtained as ~1.70 eV by $E_{mi} = E_L - E_{ex}$, which matches the energy of the second excited state ($^3T_{1g}$) from the ground state (*11*, *12*).

As a vdW antiferromagnet, $NiPS_3$ exhibits various intriguing properties and offers a unique opportunity to explore strongly correlated electron systems and magnetic systems in the 2D limit. In particular, *d-d* excitations play an important role in determining electronic and spin properties of $NiPS_3$ (*11*). Benefited from the absorption at ~1.0 eV, *d-d* transitions can be detected in bulk $NiPS_3$. However, with the reduction of the sample thickness, this absorption markedly decreases and finally becomes undetectable in atomically thin samples. The differential reflectance of few-layer $NiPS_3$ indicates the absence of clear feature at around 1.0 eV with the value approaching to zero, in contrast to the marked increase above the bandgap (see Fig. 3A). The invisibility of *d-d* excitation in atomically thin samples prevents the relative studies in 2D systems. The resonance condition enhances the signal and enables the ER scattering in $NiPS_3$, resulting to the detectable signals of *d-d* excitations in thin layers for exploring the evolution of the local electronic configuration upon thinning and stacking. As shown in Fig. 3B, the ER spectroscopy study was performed on exfoliated $NiPS_3$ layers, where the ER modes can be resolved in $NiPS_3$ from bulk down to trilayer samples, with the intensity decreasing with the reduction of layer number. Both ER modes exhibit a blue shift in the thinner samples, i.e., the energies of two *d-d* excitations increasing with the reduction of layer number (see Fig. 3C). This phenomenon indicates an increasing of crystal field splitting energy of *d* orbitals, originating from a stronger octahedral crystal field around Ni^{2+} in atomically thin samples. Furthermore, with less layer number of samples, the energy difference between two ER modes also shows a slight increase, suggesting a larger splitting of $^3T_{2g}$ state and trigonal distortion in few-layer samples.

Because of its antiferromagnetic nature, the optical properties of $NiPS_3$, such as low-frequency Raman modes and optical absorption, have showed correlations to the magnetic structure and exhibit

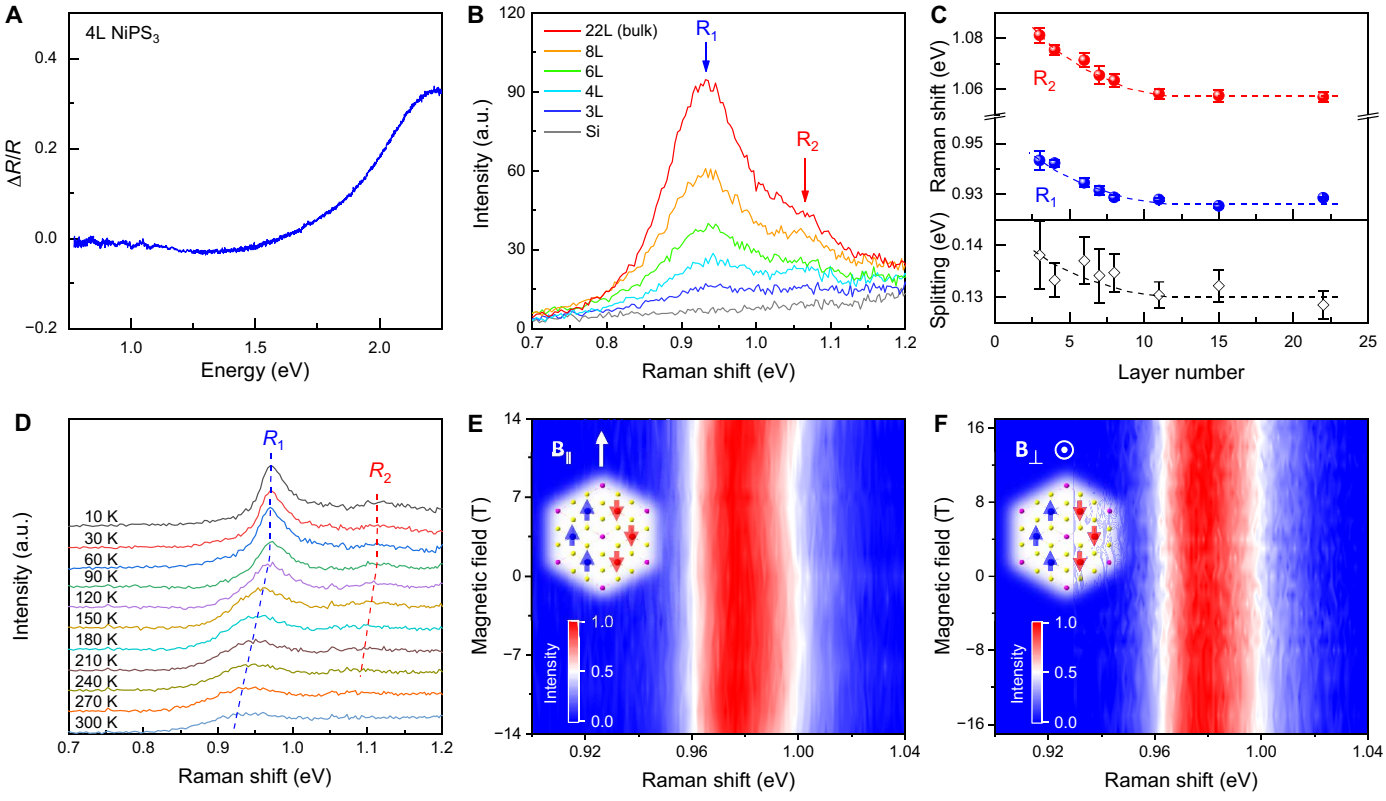

Fig. 3. Localized nature and magnetic robustness of ER modes. (**A**) Differential reflectance of a four-layer (4L) $NiPS_3$ flake. (**B**) Thickness-dependent ER spectra of $NiPS_3$ from bulk down to three-layer at 295 K. (**C**) Raman shift of two ER peaks and the energy splitting as a function of sample thickness. The evolution trends of R_1, R_2, and energy splitting are guided by the blue, red, and black dashed lines, respectively. (**D**) Temperature-dependent ER spectra of an eight-layer $NiPS_3$ flake excited by 458-nm laser from 10 to 300 K. (**E** and **F**) Color map of magnetic field–dependent ER spectra of $NiPS_3$ crystals with (E) in-plane field (along the *a* axis) $\mathbf{B}_{\parallel}$ and (F) out-of-plane field $\mathbf{B}_{\perp}$ under 488-nm laser excitation. The insets in (E) and (F) represent the directions of applied magnetic field with respect to the antiferromagnetic spin structure of $NiPS_3$.

distinct behaviors with variations of temperature and external field (*6*, *7*). Specifically, it has been demonstrated that the excitonic emission in $NiPS_3$ is strongly correlated to the spin structure, which gives rise to a distinct linear polarization of the excitonic emission (*8*–*10*, *43*). However, the correlation between spins and *d* electrons remains unexplored, especially in low-dimensional structures. To this end, the temperature-dependent ER spectroscopy measurements are conducted (see Fig. 3D). As the R_2 mode becomes hard to be resolved at low temperature due to the reduced population of the higher energy state, the following discussion related to low temperature data mainly focuses on R_1 mode. With the change of temperature from 10 to 300 K, the peak position, integrated intensity, and full width at half maximum of R_1 peak exhibit gradual variation, which could be attributed to the lattice contraction with the reduction of temperature (see fig. S5). Despite the formation of spin ordering, no marked change of the ER modes is observed across T_N. Our result indicates that the ER processes are isolated from the spin structure in $NiPS_3$, suggesting that the corresponding *d*-*d* transitions occur on a single Ni atom. In addition, it is worth noting that the ER modes have a broad peak width of tens of millielectron volts even at 10 K (see fig. S5A). Such a low temperature generally suppresses the thermal population of energy levels and results in a narrow feature of optical signals (*8*, *44*). The broad feature of ER modes can be attributed to two reasons. First, *d* orbitals of Ni^{2+} ions further split into more fine features due to the spin-orbit coupling, leading to a broad ER signal consisting of multiple electronic transitions (*11*, *41*). Second, a strong vibronic coupling is involved in the *d*-*d* transitions which are generally forbidden and requires the assistance of other media, such as phonons. As a result, ER modes are broadened due to the mismatch of nuclear coordinates (see fig. S5D). To further confirm that the *d*-*d* transitions are isolated from the spin effect, the ER study was conducted at 5 K under the external in-plane and out-of-plane magnetic fields (see Fig. 3, E and F). The results show that ER modes are also insensitive to the applied fields up to 14 T in the Voigt geometry and up to 17 T in the Faraday geometry. Since the in-plane field–induced spin-flop transition in $NiPS_3$ has been found in the magneto-PL study and isothermal magnetization measurement (*9*, *45*), the unchanged ER signal as a function of an applied in-plane field further proves that the *d*-*d* excitations are insensitive to the spin ordering in the material.

For potential opto-spintronic applications, the polarization behavior of the *d*-*d* excitations would play a substantial role. To this end, we performed a systematic polarization-resolved ER measurement on exfoliated $NiPS_3$ flakes. Both R_1 and R_2 modes exhibit stronger intensities in the parallel configuration (XX) compared to that in the cross configuration (XY) in the linear polarization study (see fig. S7A). Similarly, in the circular polarization measurement, the two ER peaks also show a stronger intensity in the parallel

configuration ($\sigma^+\sigma^+$) compared to that in the cross configuration ($\sigma^+\sigma^-$) (see fig. S7B). As a result, both ER modes in $NiPS_3$ exhibit an A_{1g} symmetry. By calculating the linear polarization degree ($\rho_l = \frac{I_{XX} - I_{XY}}{I_{XX} + I_{XY}}$) and the circular polarization degree ($\rho_c = \frac{I_{\sigma^+\sigma^+} - I_{\sigma^+\sigma^-}}{I_{\sigma^+\sigma^+} + I_{\sigma^+\sigma^-}}$), R_1 mode exhibits a $\rho_l \sim 49\%$ and a $\rho_c \sim 25\%$ at room temperature (see fig. S7C). Moreover, we further conducted a polarization angle–dependent study on $NiPS_3$ in two configurations: (I) rotating the polarization of collection light (P_{col}) with fixed polarization of incident light (P_{in}) and (II) rotating P_{in} with fixed P_{col}. Clear twofold signals emerge in the polar plot of polarization-dependent intensity of two ER modes in two configurations, in agreement with their A_{1g} symmetry (see Fig. 4, A and B). The intensities of both ER modes can be fitted by $I_{ER} = I_0 + A\cos^2\theta$, where θ is the angle between P_{in} and P_{col}; I_0 and A are fitting constants. In contrast, in the azimuthal angle–dependent study, where the sample is rotating with fixed $P_{in} \parallel P_{col}$ (configuration III), ER intensity shows independence on the crystal orientation at room temperature (see Fig. 4C). However, when the temperature goes down to 77 K, $NiPS_3$ becomes antiferromagnetic and R_1 mode exhibits an anisotropic response (see Fig. 4C). The intensity of R_1 peak can be fitted by $I_{ER} = I_1 + B\sin^2\varphi$, where φ is the angle between light polarization and the b axis of the crystal; I_1 and B are fitting constants. We define the linear polarization degree, $\rho = (I_a - I_b)/(I_a + I_b)$, where I_a (I_b) is the R_1 intensity when light polarization (both P_{in} and P_{col}) is parallel to the a (b) axis. The linear polarization degree of R_1 can be obtained ~5% at 77 K. To confirm the relation between the spin structure and the emerging polarization of R_1 mode, we conduct the temperature-dependent polarized ER measurement. The polarization degree of R_1 mode drops significantly when the temperature approaches to $T_N = 152$ K and finally disappears in the paramagnetic phase (see Fig. 4D). The temperature-dependent polarization degree in the antiferromagnetic phase is fitted well by $\rho(T) \sim \left|1 - \frac{T}{T_N}\right|^{2\beta}$, where β is a critical exponent indicating the decay trend near the phase transition temperature (*46*). We obtain $\beta = 0.27 \pm 0.03$, which is in accordance with $\beta = 0.23$ to 0.26 for the temperature-dependent magnetic intensity in 2D XY systems (*47*) and the β for the spin-induced linear polarization degree of sharp emission of $NiPS_3$ at 1.476 eV (*8*–*10*). This agreement suggests that the linear polarization of R_1 mode arises from the anisotropy of spin structure in $NiPS_3$. As a result, the polarized ER signal can serve as a probe of the magnetic phase transition in $NiPS_3$. In addition to the polarized ER measurements on a bulk sample where $T_N = 150.5 \pm 1.5$ K is obtained, we also performed similar measurements on a four-layer flake and plotted its temperature-dependent polarization degree (see fig. S10). By fitting the polarization degree at low temperature, the T_N is obtained as 150.5 ± 0.4 K, which is almost the same as the value for the bulk case. This result suggests a weak thickness dependence on the magnetic transition of $NiPS_3$ from bulk down to a four-layer region, which is in a good agreement with the previous result revealed by Raman spectroscopy (*6*). Considering the insensitivity of *d-d* transition to the spin ordering, the anisotropic ER response may be the consequence of the anisotropic absorption of incident photons due to the magnetic linear dichroism of materials, of which polarization degree is at the same order as ER response (*9*, *10*, *48*).

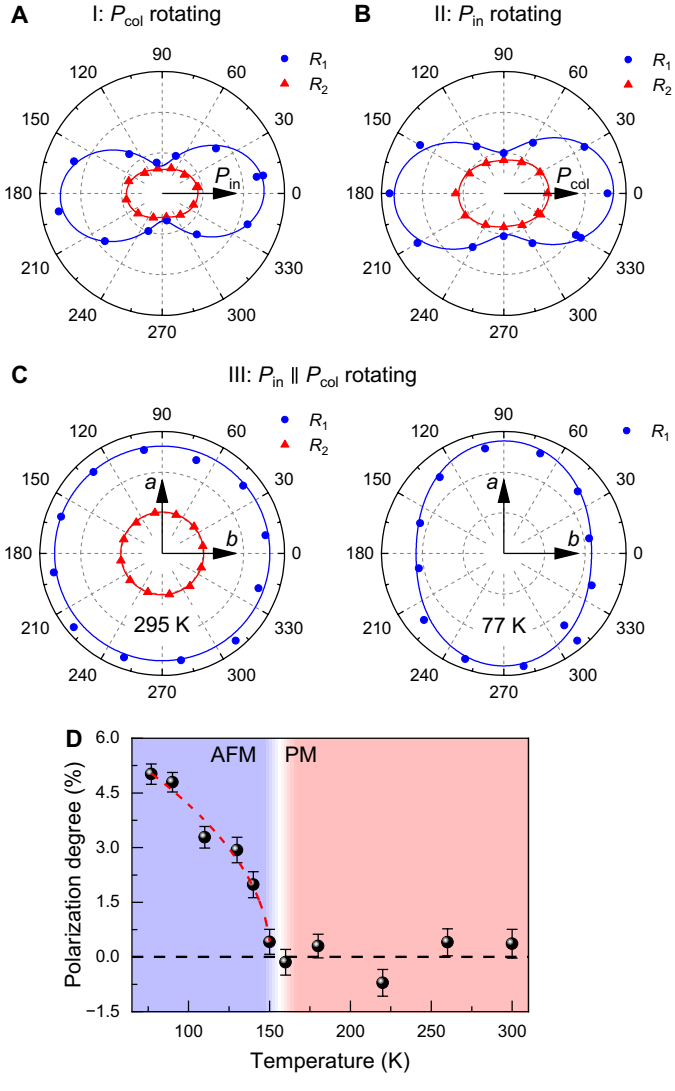

Fig. 4. Polarization-resolved ER modes in bulk $NiPS_3$ layers. (**A**) Polar plot of ER intensity of $NiPS_3$ as a function of P_{col} angle excited by 473-nm laser with fixed P_{in} (configuration I) at 295 K. (**B**) Polar plot of ER intensity of $NiPS_3$ as a function of P_{in} angle excited by 473-nm laser with fixed P_{col} (configuration II) at 295 K. (**C**) Polar plot of ER intensity of $NiPS_3$ as a function azimuthal angle excited by a 473-nm laser with $P_{in} \parallel P_{col}$ (configuration III) at 295 and 77 K. *a* and *b* axes of crystal were labeled in (C). (**D**) Polarization degree of R_1 as a function of temperature. The red dashed line is the fitting using the formula, $\rho(T) \sim \left|1 - \frac{T}{T_N}\right|^{2\beta}$, where $\beta = 0.27 \pm 0.03$.

DISCUSSION

As a correlated 2D antiferromagnet, $NiPS_3$ offers a unique opportunity to explore strongly correlated electron systems and magnetism in the 2D limit. Specifically, the investigation on *d-d* excitation is necessary in revealing various fundamental characters, such as crystal field splitting, local Hund's coupling, and Hubbard U, which are crucial for electronic structure and exchange coupling in materials. However, the forbidden selection rule of *d-d* transition raises the difficulty in its direct observation in 2D layers through absorption spectroscopy, thus prevents the fundamental study in strongly correlated electron physics in 2D limits. In this work, the *d-d* excitations are successfully probed on atomically thin $NiPS_3$ layers using ER spectroscopy. We further conduct a systematic study on *d-d* excitations, which reveals the evolution trend with the reduction of

sample thickness and the insensitivity to the spin ordering. The magnetic anisotropy origin of the linear polarized ER modes is also demonstrated. The distinct magnetic coupling of *d-d* excitations at ~1.0 eV not only offers the possibility to enrich the functions in addition to those spin-coupled electronic transition in a potential $NiPS_3$-based applications but also demonstrates the power of ER spectroscopy in the investigation of correlated 2D magnets, which could potentially open pathways to control the correlations in Mott systems.

MATERIALS AND METHODS

Sample preparation

$NiPS_3$ single crystals were grown using a chemical vapor transport method (*30*). A stoichiometric amount of high-purity elements (mole ratio Ni:P:S = 1:1:3, around 1 g in total) and iodine (about 10 to 20 mg) as a transport agent were sealed into a quartz ampule and kept in a two-zone furnace (650° to 600°C). The length of the quartz ampule is about 16 cm with a 13-mm external diameter. The pressure inside the ampule was pumped down to 1×10^{-4} torr. After 1 week of heating, the ampule was cooled down to room temperature with bulk crystals in the lower temperature end. The purity of the synthesized sample has been confirmed by series of characterizations in our previous work (*9*). Few-layer $NiPS_3$ flakes were prepared on Si substrates with 285-nm SiO_2 layers by mechanical exfoliation from a bulk single crystal.

Optical spectroscopy measurements

The ER scattering and PL measurements were carried out on a micro-Raman spectrometer (Horiba-JY T64000), and the signal was collected through a 50× long-working-distance objective. A cryostat (Cryo Industries of America, USA) was used to provide a vacuum environment and a continuous temperature from 5 to 300 K by liquid helium flow. Both ER scattering and PL measurements were performed using a single-grating mode with a grating (150 g/mm) in backscattered geometry. A series of laser lines, ranging from 454 to 568 nm, were from a Kr^+/Ar^+ ion laser (Coherent Innova 70C Spectrum) and used to excite the sample. The absorbance measurement was conducted on a spectrophotometer (Agilent Cary 5000). The polarized optical measurements were performed on another micro-Raman spectrometer (Horiba HR Evolution), and the signal was collected through a 100× objective with correction ring. The signals were dispersed with a grating (100 g/mm). A solid-state laser (λ = 473 nm) was used to excite the sample.

Magneto-PL measurements

The magneto-PL experiments were conducted in the National High Magnetic Field Laboratory. The magneto-optical experiments were performed on bulk crystal with a 14-T magnet in the Voigt geometry and a 17-T magnet in the Faraday geometry. A 488-nm continuous-wave laser was used to excite the sample. For the measurements in the Voigt geometry, the sample was vertically put inside the magnetic cell with the surface parallel to the applied magnetic field. A mirror was set between objective and sample with 45° to change the optical path by 90°. A 10× objective was used to focus the excitation laser onto the sample and also used to collect the PL signal, which subsequently past through a multimode optical fiber and was measured by a spectrometer with a charge-coupled device camera (Princeton Instruments, IsoPlane 320).

Theoretical calculations

Spin-polarized DFT calculations were carried out using the Vienna Ab Initio Simulation Package (*49*). Electron-ion interactions were described by projector augmented-wave pseudopotentials, and exchange-correlation interactions were captured by the generalized gradient approximation with the Perdew-Burke-Ernzerhof functional (*50*). To describe the strong electron correlation effects of localized Ni 3*d* orbitals in $NiPS_3$, a simplified (rotationally invariant) DFT + U_{eff} approach (*51*) was adopted with an effective *U* parameter of 4.0 eV, a common value used in previous studies (*6*, *7*, *9*). The DFT-D3 method was used for considering the vdW interactions between the layers (*52*). The lattice constants and atomic positions of bulk $NiPS_3$ were both relaxed until the residual forces were below 0.01 eV/Å, where the cutoff energy was set at 350 eV and the Γ-centered *K*-point mesh was 12 × 6 × 12. Initial magnetic moments of 4 or −4 were chosen for each Ni atom in the experimental zigzag antiferromagnetic order.

SUPPLEMENTARY MATERIALS

Supplementary material for this article is available at https://science.org/doi/10.1126/sciadv.abl7707

REFERENCES AND NOTES

1. B. Huang, G. Clark, E. Navarro-Moratalla, D. R. Klein, R. Cheng, K. L. Seyler, D. Zhong, E. Schmidgall, M. A. McGuire, D. H. Cobden, W. Yao, D. Xiao, P. Jarillo-Herrero, X. Xu, Layer-dependent ferromagnetism in a van der Waals crystal down to the monolayer limit. *Nature* **546**, 270–273 (2017).
2. C. Gong, L. Li, Z. Li, H. Ji, A. Stern, Y. Xia, T. Cao, W. Bao, C. Wang, Y. Wang, Z. Q. Qiu, R. J. Cava, S. G. Louie, J. Xia, X. Zhang, Discovery of intrinsic ferromagnetism in two-dimensional van der Waals crystals. *Nature* **546**, 265–269 (2017).
3. K. S. Burch, D. Mandrus, J.-G. Park, Magnetism in two-dimensional van der Waals materials. *Nature* **563**, 47–52 (2018).
4. C. Gong, X. Zhang, Two-dimensional magnetic crystals and emergent heterostructure devices. *Science* **363**, eaav4450 (2019).
5. B. Huang, M. A. McGuire, A. F. May, D. Xiao, P. Jarillo-Herrero, X. Xu, Emergent phenomena and proximity effects in two-dimensional magnets and heterostructures. *Nat. Mater.* **19**, 1276–1289 (2020).
6. K. Kim, S. Y. Lim, J.-U. Lee, S. Lee, T. Y. Kim, K. Park, G. S. Jeon, C.-H. Park, J.-G. Park, H. Cheong, Suppression of magnetic ordering in XXZ-type antiferromagnetic monolayer $NiPS_3$. *Nat. Commun.* **10**, 345 (2019).
7. S. Y. Kim, T. Y. Kim, L. J. Sandilands, S. Sinn, M.-C. Lee, J. Son, S. Lee, K. Y. Choi, W. Kim, B.-G. Park, C. Jeon, H.-D. Kim, C.-H. Park, J.-G. Park, S. J. Moon, T. W. Noh, Charge-spin correlation in van der Waals antiferromagnet $NiPS_3$. *Phys. Rev. Lett.* **120**, 136402 (2018).
8. S. Kang, K. Kim, B. H. Kim, J. Kim, K. I. Sim, J. U. Lee, S. Lee, K. Park, S. Yun, T. Kim, A. Nag, A. Walters, M. Garcia-Fernandez, J. Li, L. Chapon, K. J. Zhou, Y. W. Son, J. H. Kim, H. Cheong, J. G. Park, Coherent many-body exciton in van der Waals antiferromagnet $NiPS_3$. *Nature* **583**, 785–789 (2020).
9. X. Wang, J. Cao, Z. Lu, A. Cohen, H. Kitadai, T. Li, Q. Tan, M. Wilson, C. H. Lui, D. Smirnov, S. Sharifzadeh, X. Ling, Spin-induced linear polarization of photoluminescence in antiferromagnetic van der Waals crystals. *Nat. Mater.* **20**, 964–970 (2021).
10. K. Hwangbo, Q. Zhang, Q. Jiang, Y. Wang, J. Fonseca, C. Wang, G. M. Diederich, D. R. Gamelin, D. Xiao, J.-H. Chu, W. Yao, X. Xu, Highly anisotropic excitons and multiple phonon bound states in a van der Waals antiferromagnetic insulator. *Nat. Nanotechnol.* **16**, 655–660 (2021).
11. D. Afanasiev, J. R. Hortensius, M. Matthiesen, S. Mañas-Valero, M. Šiškins, M. Lee, E. Lesne, H. S. J. van der Zant, P. G. Steeneken, B. A. Ivanov, E. Coronado, A. D. Caviglia, Controlling the anisotropy of a van der Waals antiferromagnet with light. *Sci. Adv.* **7**, eabf3096 (2021).
12. C. A. Belvin, E. Baldini, I. O. Ozel, D. Mao, H. C. Po, C. J. Allington, S. Son, B. H. Kim, J. Kim, I. Hwang, J. H. Kim, J.-G. Park, T. Senthil, N. Gedik, Exciton-driven antiferromagnetic metal in a correlated van der Waals insulator. *Nat. Commun.* **12**, 4837 (2021).
13. L. J. Sandilands, Y. Tian, A. A. Reijnders, H.-S. Kim, K. W. Plumb, Y.-J. Kim, H.-Y. Kee, K. S. Burch, Spin-orbit excitations and electronic structure of the putative Kitaev magnet α-$RuCl_3$. *Phys. Rev. B* **93**, 075144 (2016).
14. K. L. Seyler, D. Zhong, D. R. Klein, S. Gao, X. Zhang, B. Huang, E. Navarro-Moratalla, L. Yang, D. H. Cobden, M. A. McGuire, W. Yao, D. Xiao, P. Jarillo-Herrero, X. Xu, Ligand-field helical luminescence in a 2D ferromagnetic insulator. *Nat. Phys.* **14**, 277–281 (2018).

15. J.-H. Lee, Y. Choi, S.-H. Do, B. H. Kim, M.-J. Seong, K.-Y. Choi, Multiple spin-orbit excitons in α-$RuCl_3$ from bulk to atomically thin layers. *npj Quantum Mater.* **6**, 43 (2021).
16. J. van den Brink, G. A. Sawatzky, Non-conventional screening of the Coulomb interaction in low-dimensional and finite-size systems. *Europhys. Lett.* **50**, 447–453 (2000).
17. P. H. Tan, W. P. Han, W. J. Zhao, Z. H. Wu, K. Chang, H. Wang, Y. F. Wang, N. Bonini, N. Marzari, N. Pugno, G. Savini, A. Lombardo, A. C. Ferrari, The shear mode of multilayer graphene. *Nat. Mater.* **11**, 294–300 (2012).
18. C. Lee, H. Yan, L. E. Brus, T. F. Heinz, J. Hone, S. Ryu, Anomalous lattice vibrations of single- and few-layer MoS_2. *ACS Nano* **4**, 2695–2700 (2010).
19. Y. Wang, G. B. Osterhoudt, Y. Tian, P. Lampen-Kelley, A. Banerjee, T. Goldstein, J. Yan, J. Knolle, H. Ji, R. J. Cava, J. Nasu, Y. Motome, S. E. Nagler, D. Mandrus, K. S. Burch, The range of non-Kitaev terms and fractional particles in α-$RuCl_3$. *npj Quantum Mater.* **5**, 14 (2020).
20. X. Wang, K. Du, Y. Y. F. Liu, P. Hu, J. Zhang, Q. Zhang, M. H. S. Owen, X. Lu, C. K. Gan, P. Sengupta, C. Kloc, Q. Xiong, Raman spectroscopy of atomically thin two-dimensional magnetic iron phosphorus trisulfide ($FePS_3$) crystals. *2D Mater.* **3**, 031009 (2016).
21. J.-U. Lee, S. Lee, J. H. Ryoo, S. Kang, T. Y. Kim, P. Kim, C.-H. Park, J.-G. Park, H. Cheong, Ising-type magnetic ordering in atomically thin $FePS_3$. *Nano Lett.* **16**, 7433–7438 (2016).
22. T. Yao, J. G. Mason, J. Huiwen, R. J. Cava, S. B. Kenneth, Magneto-elastic coupling in a potential ferromagnetic 2D atomic crystal. *2D Mater.* **3**, 025035 (2016).
23. Z. Liu, K. Guo, G. Hu, Z. Shi, Y. Li, L. Zhang, H. Chen, L. Zhang, P. Zhou, H. Lu, M.-L. Lin, S. Liu, Y. Cheng, X. L. Liu, J. Xie, L. Bi, P.-H. Tan, L. Deng, C.-W. Qiu, B. Peng, Observation of nonreciprocal magnetophonon effect in nonencapsulated few-layered CrI_3. *Sci. Adv.* **6**, eabc7628 (2020).
24. B. Huang, J. Cenker, X. Zhang, E. L. Ray, T. Song, T. Taniguchi, K. Watanabe, M. A. McGuire, D. Xiao, X. Xu, Tuning inelastic light scattering via symmetry control in the two-dimensional magnet CrI3. *Nat. Nanotechnol.* **15**, 212–216 (2020).
25. H. Farhat, S. Berciaud, M. Kalbac, R. Saito, T. F. Heinz, M. S. Dresselhaus, J. Kong, Observation of electronic raman scattering in metallic carbon nanotubes. *Phys. Rev. Lett.* **107**, 157401 (2011).
26. B. Fluegel, A. V. Mialitsin, D. A. Beaton, J. L. Reno, A. Mascarenhas, Electronic Raman scattering as an ultra-sensitive probe of strain effects in semiconductors. *Nat. Commun.* **6**, 7136 (2015).
27. C. Lane, J.-X. Zhu, Thickness dependence of electronic structure and optical properties of a correlated van der Waals antiferromagnetic $NiPS_3$ thin film. *Phys. Rev. B* **102**, 075124 (2020).
28. P. A. Joy, S. Vasudevan, Magnetism in the layered transition-metal thiophosphates MPS_3 (M = Mn, Fe, and Ni). *Phys. Rev. B* **46**, 5425–5433 (1992).
29. A. R. Wildes, V. Simonet, E. Ressouche, G. J. McIntyre, M. Avdeev, E. Suard, S. A. J. Kimber, D. Lançon, G. Pepe, B. Moubaraki, T. J. Hicks, Magnetic structure of the quasi-two-dimensional antiferromagnet $NiPS_3$. *Phys. Rev. B* **92**, 224408 (2015).
30. K.-z. Du, X.-z. Wang, Y. Liu, P. Hu, M. Iqbal Bakti Utama, C. K. Gan, Q. Xiong, C. Kloc, Weak van der Waals stacking, wide-range band gap, and raman study on ultrathin layers of metal phosphorus trichalcogenides. *ACS Nano* **10**, 1738–1743 (2016).
31. T. P. Devereaux, R. Hackl, Inelastic light scattering from correlated electrons. *Rev. Mod. Phys.* **79**, 175–233 (2007).
32. C.-T. Kuo, M. Neumann, K. Balamurugan, H. J. Park, S. Kang, H. W. Shiu, J. H. Kang, B. H. Hong, M. Han, T. W. Noh, J.-G. Park, Exfoliation and Raman spectroscopic fingerprint of few-layer $NiPS_3$ van der Waals crystals. *Sci. Rep.* **6**, 20904 (2016).
33. M. Scagliotti, M. Jouanne, M. Balkanski, G. Ouvrard, G. Benedek, Raman-scattering in antiferromagnetic $FePS_3$ and $FePSe_3$ crystals. *Phys. Rev. B* **35**, 7097–7104 (1987).
34. C.-T. Kuo, K. Balamurugan, H. W. Shiu, H. J. Park, S. Sinn, M. Neumann, M. Han, Y. J. Chang, C.-H. Chen, H.-D. Kim, J.-G. Park, T. W. Noh, The energy band alignment at the interface between mechanically exfoliated few-layer NiPS3 nanosheets and ZnO. *Curr. Appl. Phys.* **16**, 404–408 (2016).
35. M. Piacentini, F. S. Khumalo, C. G. Olson, J. W. Anderegg, D. W. Lynch, Optical transitions, XPS, electronic states in $NiPS_3$. *Chem. Phys.* **65**, 289–304 (1982).
36. M. Abramchuk, S. Jaszewski, K. R. Metz, G. B. Osterhoudt, Y. Wang, K. S. Burch, F. Tafti, Controlling magnetic and optical properties of the van der Waals crystal CrCl3−xBrx via mixed halide chemistry. *Adv. Mater.* **30**, 1801325 (2018).
37. M. Wu, Z. Li, T. Cao, S. G. Louie, Physical origin of giant excitonic and magneto-optical responses in two-dimensional ferromagnetic insulators. *Nat. Commun.* **10**, 2371 (2019).
38. G. Kotliar, S. Y. Savrasov, K. Haule, V. S. Oudovenko, O. Parcollet, C. A. Marianetti, Electronic structure calculations with dynamical mean-field theory. *Rev. Mod. Phys.* **78**, 865–951 (2006).
39. H. Park, A. J. Millis, C. A. Marianetti, Computing total energies in complex materials using charge self-consistent DFT + DMFT. *Phys. Rev. B* **90**, 235103 (2014).
40. R. Liu, D. Salamon, M. V. Klein, S. L. Cooper, W. C. Lee, S.-W. Cheong, D. M. Ginsberg, Novel Raman-active electronic excitations near the charge-transfer gap in insulating cuprates. *Phys. Rev. Lett.* **71**, 3709–3712 (1993).
41. M. L. Sanjuan, M. A. Kanehisa, M. Jouanne, Electronic Raman study of Fe^{2+} in $FeP\mathit{X}_3$ (X=S,Se) layered compounds. *Phys. Rev. B* **46**, 11501–11506 (1992).
42. J. R. Ferraro, K. Nakamoto, C. W. Brown, *Introductory Raman Spectroscopy* (Elsevier, 2003), vol. 1.
43. C.-H. Ho, T.-Y. Hsu, L. C. Muhimmah, The band-edge excitons observed in few-layer $NiPS_3$. *npj 2D Mater. Appl.* **5**, 8 (2021).
44. F. Cadiz, E. Courtade, C. Robert, G. Wang, Y. Shen, H. Cai, T. Taniguchi, K. Watanabe, H. Carrere, D. Lagarde, M. Manca, T. Amand, P. Renucci, S. Tongay, X. Marie, B. Urbaszek, Excitonic linewidth approaching the homogeneous limit in MoS_2-Based van der Waals heterostructures. *Phys. Rev. X* **7**, 021026 (2017).
45. R. Basnet, A. Wegner, K. Pandey, S. Storment, J. Hu, Highly sensitive spin-flop transition in antiferromagnetic van der Waals material $M\mathrm{PS}_3$ (M=Ni and Mn). *Phys. Rev. Mater.* **5**, 064413 (2021).
46. J. Ferre, G. A. Gehring, Linear optical birefringence of magnetic crystals. *Rep. Prog. Phys.* **47**, 513–611 (1984).
47. S. T. Bramwell, P. C. W. Holdsworth, Magnetization and universal sub-critical behaviour in two-dimensional XY magnets. *J. Phys. Condens. Matter* **5**, L53–L59 (1993).
48. Q. Zhang, K. Hwangbo, C. Wang, Q. Jiang, J.-H. Chu, H. Wen, D. Xiao, X. Xu, Observation of giant optical linear dichroism in a zigzag antiferromagnet $FePS_3$. *Nano Lett.* **21**, 6938–6945 (2021).
49. G. Kresse, J. Furthmüller, Efficiency of ab-initio total energy calculations for metals and semiconductors using a plane-wave basis set. *Comput. Mater. Sci.* **6**, 15–50 (1996).
50. J. P. Perdew, K. Burke, M. Ernzerhof, Generalized gradient approximation made simple. *Phys. Rev. Lett.* **77**, 3865–3868 (1996).
51. S. L. Dudarev, G. A. Botton, S. Y. Savrasov, C. J. Humphreys, A. P. Sutton, Electron-energy-loss spectra and the structural stability of nickel oxide: An LSDA+U study. *Phys. Rev. B* **57**, 1505–1509 (1998).
52. S. Grimme, J. Antony, S. Ehrlich, H. Krieg, A consistent and accurate ab initio parametrization of density functional dispersion correction (DFT-D) for the 94 elements H-Pu. *J. Chem. Phys.* **132**, 154104 (2010).

Acknowledgments

Funding: This material is based upon work supported by the National Science Foundation (NSF) under grant no. 1945364. X.W. and X.L. acknowledge the financial support from Boston University. X.L. acknowledges the membership of the Boston University Photonics Center. L.L. acknowledges computational resources of the Compute and Data Environment for Science (CADES) at the Oak Ridge National Laboratory, which is supported by the Office of Science of the U.S. Department of Energy under contract no. DE-AC05-00OR22725. A portion of this research (DFT calculations) used resources at the Center for Nanophase Materials Sciences, which is a U.S. Department of Energy Office of Science User Facility. A.C., A.H., and S.S. acknowledge financial support from the U.S. Department of Energy (DOE), Office of Science, Basic Energy Sciences (BES) Early Career Program under award no. DESC0018080. We acknowledge the computational resources through the Extreme Science and Engineering Discovery Environment (XSEDE), which is supported by National Science Foundation grant number ACI-1548562, and the National Energy Research Scientific Computing Center, a DOE Office of Science User Facility supported by the Office of Science of the U.S. Department of Energy under contract no. DE-AC02-05CH11231. W.X. acknowledges the National Natural Science Foundation of China (21873048) and the Natural Science Foundation of Jiangsu Province (BK20180319). Z.L. and D.S. acknowledge support from the U.S. Department of Energy (no. DE-FG02-07ER46451) for high-field magnetospectroscopy measurements performed at National High Magnetic Field Laboratory, which is supported by the National Science Foundation through NSF/DMR-1644779 and the state of Florida. K.S.B. is grateful for the support of the Office of Naval Research under award number N00014-20-1-2308.

Author contributions: X.W. and X.L. conceived the project. X.W., J.C., H.L., and Z.L. performed the optical spectroscopy experiment under the supervision of D.S., W.X., and X.L. J.C. and Q.T. synthesized the bulk $NiPS_3$ crystal. X.W., H.K., and Q.T. prepared and characterized the exfoliated samples. A.C., A.H., S.S., and L.L. performed theoretical calculations. X.W. and X.L. performed the analysis and interpretation of the data with the significant input from K.S.B., S.S., and L.L. X.W. and X.L. wrote the manuscript with contributions from all authors.

Competing interests: The authors declare that they have no competing interests. **Data and materials availability:** All data needed to evaluate the conclusions in the paper are present in the paper and/or the Supplementary Materials.

Submitted 4 August 2021
Accepted 22 November 2021
Published 14 January 2022
10.1126/sciadv.abl7707

ScienceAdvances

Electronic Raman scattering in the 2D antiferromagnet NiPS

Xingzhi WangJun CaoHua LiZhengguang LuArielle CohenAnubhab HaldarHikari KitadaiQishuo TanKenneth S. BurchDmitry SmirnovWeigao XuSahar SharifzadehLiangbo LiangXi Ling

Sci. Adv., 8 (2), eabl7707. • DOI: 10.1126/sciadv.abl7707

Science Advances (ISSN) is published by the American Association for the Advancement of Science. 1200 New York Avenue NW, Washington, DC 20005. The title *Science Advances* is a registered trademark of AAAS.